AIAA JOURNAL
Vol. 44, No. 2, February 2006

Flame Acceleration in Narrow Channels: Applications for Micropropulsion in Low-Gravity Environments

Vadim N. Gamezo* and Elaine S. Oran†
Naval Research Laboratory, Washington, D.C. 20375

A laminar flame propagating toward the open end of a narrow channel filled with a gaseous combustible mixture can accelerate or oscillate, depending on the wall temperature and the channel width. The accelerating flame is able to produce a high-speed flow that has the potential to provide significant thrust. We study these phenomena using multidimensional reactive Navier–Stokes numerical simulations, and show that for adiabatic walls, the maximum flame acceleration occurs when the the channel is about five times larger than the reaction zone of a laminar flame. In three-dimensional square channels, the flame speed increases roughly two times faster than in two-dimensional channels. The accelerating flame generates weak compression waves that propagate with a local sound speed and can accelerate the unreacted material ahead of the flame to velocities close to the speed of sound without creating strong shocks. This combustion regime is of particular interest for micropropulsion because it allows efficient use of fuel and gradual development of thrust.

I. Introduction

THIS work is based on a micropropulsion idea generated from a relatively recent discovery concerning the behavior of laminar flames propagating in very narrow tubes. When a slow laminar flame is ignited near the closed end of a tube, the material ahead of the flame is accelerated and a boundary layer is formed along the walls in the unreacted material. Due to the presence of the boundary layer, the flow velocity changes across the channel, increasing from zero at the wall to a maximum in the middle of the tube. Previous simulations[1–3] have shown that the nonuniform flow stretches the flame, so that the shape of the flame becomes similar to the velocity profile. This increases the flame surface area, thus accelerating the energy generation and the flow. There is little change in the laminar burning rate, but the speed of the flame that propagates with the flow grows very rapidly in the laboratory frame of reference, from centimeters per second to hundreds of meters per second for adiabatic walls.

This flame-acceleration phenomenon, explained by Ott[1] and Ott et al.,[2,3] is different from the well-known case of flame propagation in a channel with cold walls where the flame quenches near the walls, and the flame velocity oscillates. These oscillating flames were originally reported in the classical work of Mallard and Le Chatelier[4] and recently studied in experiments.[5,6] Flame propagation in adiabatic and nonadibatic channels was also studied in recent theoretical and numerical work.[7–9]

Here we consider regimes in which the flame propagating in a narrow channel remains laminar, and no strong shocks or detonations are present. Such regimes are of particular interest for micropropulsion because the high-speed flow created by the accelerating flame could provide significant thrust that could be further enhanced by attaching an appropriately shaped exit nozzle. The thrust would gradually increase as the flame and flow accelerated, and reach a maximum when the flame approached the open end of the tube or the nozzle. In contrast to the majority of other combustion-based propulsion concepts, most of the thrust here can be provided by material accelerated ahead of the flame. Therefore, a propulsion device could only be partially filled with a combustible mixture. The rest of the material can be an inert gas or combustion products from a previous pulse.

This micropropulsion concept is of particular interest for low-gravity environments, where relatively small, controlled thrusts could be used for navigational corrections. In such cases, there might not be a need for the high repetition rates required for pulse combustion and pulse detonation engines.

The purpose of this paper is to confirm original results[1–3] and to carry the study further to examine the possibility of using flame acceleration in narrow tubes for micropropulsion. As a model energetic system, we consider the same stoichiometric acetylene-oxygen mixture used in Ref. 3, perform numerical simulations for two-dimensional and three-dimensional channels of different widths and lengths, and analyze effects of channel sizes on integral propulsion characteristics.

II. Numerical Model Development

The basic idea of this work comes from previous computational studies[1–3] carried out with a fully compressible reactive fluid dynamics code that used a high-order flux-corrected transport algorithm and a uniform mesh. The code was implemented on a massively parallel computer with a special architecture that has since become obsolete.

Therefore, the first step in this new project was to reproduce selected computations with the latest computational technology, suitable for parallel computations on currently available computers. Now we are using an explicit, second-order, Godunov-type code[10,11] that solves reactive Navier–Stokes equations:

$$\frac{\partial \rho}{\partial t} = -\nabla \cdot (\rho \boldsymbol{U})$$

$$\frac{\partial (\rho \boldsymbol{U})}{\partial t} = -\nabla \cdot (\rho \boldsymbol{U}\boldsymbol{U}) - \nabla P - \nabla \cdot \hat{\tau}$$

$$\frac{\partial E}{\partial t} = -\nabla \cdot [(E + P)\boldsymbol{U}] - \nabla \cdot (\boldsymbol{U} \cdot \hat{\tau}) - \nabla \cdot (K \nabla T) - \rho q \dot{w} \quad (1)$$

$$\frac{\partial (\rho Y)}{\partial t} = -\nabla \cdot (\rho Y \boldsymbol{U}) - \nabla \cdot (\rho D \nabla Y) + \rho \dot{w}$$

Here ρ is the mass density, $\boldsymbol{U}$ is the fluid velocity vector, E is the energy density, P is the pressure, Y is the unburned mass fraction, K is the thermal conduction coefficient, D is the mass diffusion

Presented as Paper 2005-0540 at the 43rd Aerospace Sciences Meeting, Reno, NV, 10–13 January 2005; received 4 March 2005; revision received 19 July 2005; accepted for publication 5 September 2005.

*Research Physicist, Laboratory for Computational Physics and Fluid Dynamics. Member AIAA.
†Senior Scientist for Reactive Flow Physics, Laboratory for Computational Physics and Fluid Dynamics. Fellow AIAA.

coefficient, q is the chemical energy release, and $\dot{w}$ is the reaction source term. The viscous stress tensor is defined as

$$\hat{\tau} = \rho\nu\left[\tfrac{2}{3}(\nabla\cdot\boldsymbol{U})\hat{I} - (\nabla\boldsymbol{U}) - (\nabla\boldsymbol{U})^{\dagger}\right] \tag{2}$$

where ν is the kinematic shear viscosity, $\hat{I}$ is a unit matrix, and the superscript † indicates matrix transposition.

The equation of state is that of an ideal gas,

$$P = \rho RT/M, \qquad E = P/(\gamma-1) + \rho U^2/2 \tag{3}$$

where γ is the adiabatic index, R is the universal gas constant, and M is the molecular weight. The chemical source term describes first-order Arrhenius kinetics:

$$\frac{\mathrm{d}Y}{\mathrm{d}t} \equiv \dot{w} = -A\rho Y \exp\left(-\frac{Q}{RT}\right) \tag{4}$$

where A is the preexponential factor and Q is the activation energy. Taking the reaction rate $\dot{w}$ proportional to ρ accounts for the binary nature of chemical reactions taking place in real combustion systems.

Molecular transport coefficients are functions of temperature:

$$\nu = \nu_0(T^n/\rho), \qquad D = D_0(T^n/\rho), \qquad K/\rho C_p = \kappa_0(T^n/\rho) \tag{5}$$

where ν_0, D_0, and κ_0 are constants, $C_p = \gamma R/M(\gamma-1)$ is the specific heat at constant pressure, and $n = 0.7$ models the temperature dependence typical of these coefficients in reactive hydrocarbon systems.

The equations are solved on a dynamically adapting Cartesian structured mesh using a direction-splitting approach for multidimensional solutions. The adaptive mesh refinement (AMR) increases numerical resolution in the vicinity of important flow features, such as flame fronts, shocks, and boundary layers, reduces the computing time for two-dimensional simulations, and allows us to solve the problem in three dimensions in a reasonable amount of time. This code has been extensively tested on a variety of combustion problems,[11–15] including flame–shock interactions and boundary-layer effects. The code was modified for this project to incorporate additional calculations of integral propulsion characteristics, such as mass outflow, thrust, and specific impulse.

We have performed a series of resolution and mesh-refinement tests and tuned the AMR to make sure that the important flow features are well resolved. The simulations were carried out using two levels of mesh refinement with the fine mesh applied in the vicinity of the flame front. The cell sizes for these two levels differ by a factor of 2. The minimum computational cell size was varied from 0.002 cm for larger channels to 0.0005 cm for smaller channels to ensure an adequate resolution of velocity gradients. The computational results obtained for different numerical resolutions are compared in the next section.

We then considered a model for the same energetic system (a low-pressure stoichiometric acetylene–oxygen mixture defined in Table 1), the same geometry (shown in Fig. 1), and the same boundary conditions (adiabatic wall) used in the original study.[3] The results show and thus confirm the same mechanism of flame acceleration induced by the boundary-layer effect. Therefore, even though there is still no direct experimental evidence for this mechanism, the existence of the phenomenon has been confirmed by two independent numerical codes that implement the same physical model in two different ways.

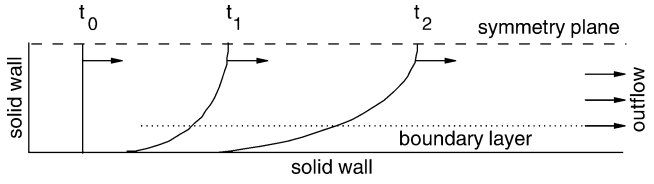

Fig. 1 Problem geometry. The flame front is shown at the initial time t_0 and at later times t_1 and t_2.

Table 1 Material and chemistry parameters for stoichiometric acetylene–air mixture

Parameter	Value	Definition
T_0	293 K	Initial temperature
P_0	1.33×10^5 erg/cm^3	Initial pressure
ρ_0	1.58×10^{-4} g/cm^3	Initial density
γ	1.25	Adiabatic index
M	29 g/mol	Molecular weight
A	10^{12} cm^3/g · s	Preexponential factor
Q	$29.3\,R\,T_0$	Activation energy
q	$35.0\,R\,T_0/M$	Chemical energy release
$\nu_0=\mu_0=D_0$	1.3×10^{-6} g/s · cm · K$^{0.7}$	Transport constants in Eq. (5)

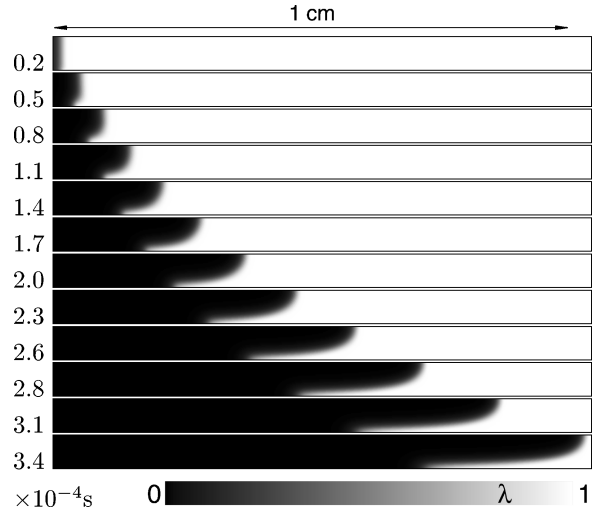

Fig. 2 Time sequence of unburned mass fraction plots showing the evolution of a laminar flame in two-dimensional half-channel for $L = 1.024$ cm and $d/2 = 0.064$ cm. The minimum computational cell size is 0.001 cm.

III. Two-Dimensional Results

The problem geometry is similar to that used in Ref. 3 and is shown in Fig. 1. We modeled half of a channel, applying a no-slip reflecting boundary condition at $x = 0$ and a symmetry condition at $d/2$, where d is the channel width. Two channel lengths L were considered: 1.024 and 8.192 cm. The channel width d was varied from 0.0128 to 1.024 cm, or from 1 to 80 in units of the laminar flame thickness x_l defined below.

The channel was filled with a low-pressure (100-Torr) stoichiometric acetylene–oxygen mixture, parameters for which are defined in Table 1. The laminar flame speed for this mixture is 1.53 m/s. The laminar flame thickness x_l, defined as the distance between the planes $Y = 0.2$ and $Y = 0.8$, is 0.0128 cm. This value is about two times smaller than the flame thickness defined through the maximum temperature gradient and used in Ref. 3.

A planar laminar flame was ignited near the closed end of the channel by placing a 0.01-cm-thick layer of hot burned material at adiabatic flame temperature near the left boundary. The initial discontinuity between burned and unburned materials was spread by molecular diffusion, heat conduction, and chemical reaction and evolved into a self-consistent flame during the first few thousand timesteps, or about 0.2×10^{-4} s of physical time.

Details of the flame evolution for $L = 1.024$ cm and $d/x_l = 10$ are shown in Fig. 2. The flame propagation in this narrow channel is affected by the velocity gradient in a boundary layer that forms along the wall ahead of the flame. This boundary layer develops in the flow of unburned material induced by the expansion of the burning gas. As the boundary layer forms, the flow velocity changes across the channel, increasing from zero at the wall to a maximum in the middle of the tube. The nonuniform flow stretches the flame so that the shape of the flame becomes similar to the velocity profile. This increases the flame surface area, thus accelerating the energy

generation and the flow. There is little change in the laminar burning rate, but the speed of the flow ahead of the flame, and the speed of the flame that propagates with the flow, grow rapidly in the laboratory frame of reference to about 55 m/s at the end of the channel, as shown in Fig. 3. The curves in Fig. 3 correspond to three different numerical resolutions used in this paper and show only a minor resolution effect on the outflow velocity.

A typical calculated flowfield in the vicinity of the accelerating flame in Fig. 2 is shown in Fig. 4. The flow features include the curved flame surface, the boundary layer near the bottom wall, the fast-moving unburned material ahead of the flame, the relatively slow-moving burned material behind the flame, and the velocity gradient inside the tip of the flame that ensures the growth of the flame surface area. These results show the same mechanism of flame acceleration induced by the boundary-layer effect as was reported in Refs. 1–3.

We repeated the simulations for different channel widths and a constant $L = 1.024$ cm. Figure 5 shows the maximum outlow velocity as a function of scaled channel width. For channel widths comparable to the flame thickness, $d \sim x_l$, the flame remains practically one-dimensional for the entire time it travels down the channel. As d becomes larger, however, so that $d > 2x_l$, boundary layers begin to affect the flow, and the flame and flow velocities increase. The maximum flame acceleration occurs for $d/x_l = 5$, and the outflow velocity in this case reaches 100 m/s. For wider channels, the flame acceleration decreases because the part of the flame surface initially affected by the developing boundary layer is smaller, and the maximum outflow velocity for a fixed channel length decreases.

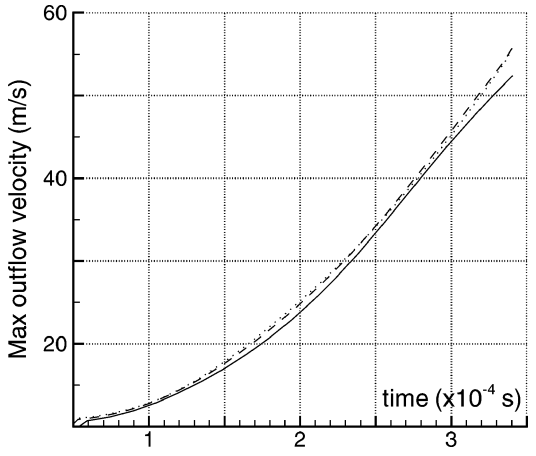

Fig. 3 Maximum outflow velocity at the right boundary calculated for two-dimensional half-channel 1.024 × 0.064 cm for different numerical resolutions. Minimum computational cell sizes: ——, 0.002; - - - -, 0.001; and · · · ·, 0.0005 cm.

In longer channels, where the flame and the boundary layer have more time to develop, the flow can eventually accelerate to the sound speed. For example, the simulations performed for $L = 8.192$ cm and $d/x_l = 5$ predict the maximum outflow velocity 370 m/s, which is close to the sound speed in the unburned material. A time sequence of pressure and flow velocity profiles for this case is shown in Fig. 6. The pressure and velocity increase between the open end of the channel ($x = 8.192$ cm) and the flame, and then drop in the reaction zone. The velocity becomes negative, and then increases to 0 at the closed end ($x = 0$) as the boundary condition requires. The pressure slightly decreases in the reaction zone and behind the flame, but it is still high enough to reverse the flow in positive direction at later times, after the flame reaches the open end.

Pressure, velocity, and their gradients ahead of the flame increase with time because of compression waves generated by the energy release. In a longer channel or in a more energetic system, the compression waves may converge to a strong shock, but this does not occur for the reactive mixture and channel sizes considered here.

IV. Three-Dimensional Results

The computational setup for three-dimensional simulations was similar to the two-dimensional geometry shown in Fig. 1. The computational domain covered a quarter of a square channel and was bounded by no-slip adiabatic walls at $y = 0$ and $z = 0$ and symmetry boundaries at y and $z = d/2$. We considered four channel lengths, 1.024, 2.048, 4.096, and 8.192 cm, and varied the scaled channel width d/x_l from 2.5 to 20. We used the same reactive mixture as for two-dimensional simulation. Simulations were stopped when the flame reached the open end of the channel.

The evolution of the full three-dimensional flame surface for $L = 1.024$ cm and $d/x_l = 5$, 10, and 20 is shown in Fig. 7. For

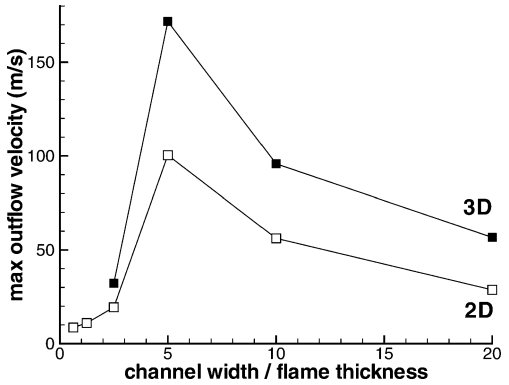

Fig. 5 Maximum outflow velocity calculated for the fixed channel length 1.024 cm as a function of channel width scaled by the laminar flame thickness 0.0128 cm.

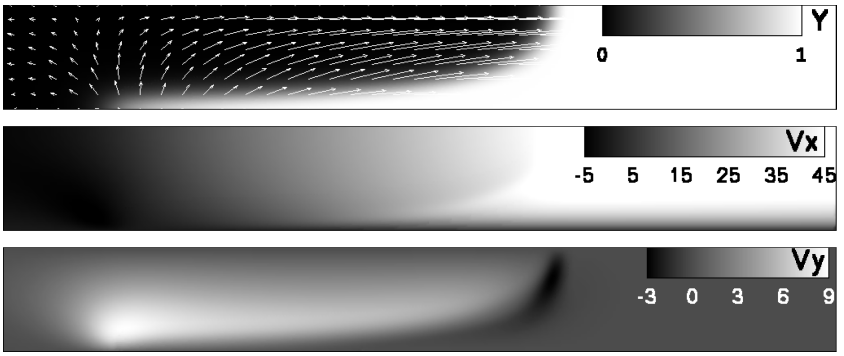

Fig. 4 Unburned mass fraction Y with superimposed velocity vectors, longitudinal velocity V_x, and transverse velocity V_y, in the vicinity of an accelerating flame in two-dimensional half-channel 1.024 × 0.064 cm. Shown is the part of the computational domain 0.5 × 0.064 cm adjacent to the right (outflow) boundary. Time 3.1 × 10^{-4} s after ignition.

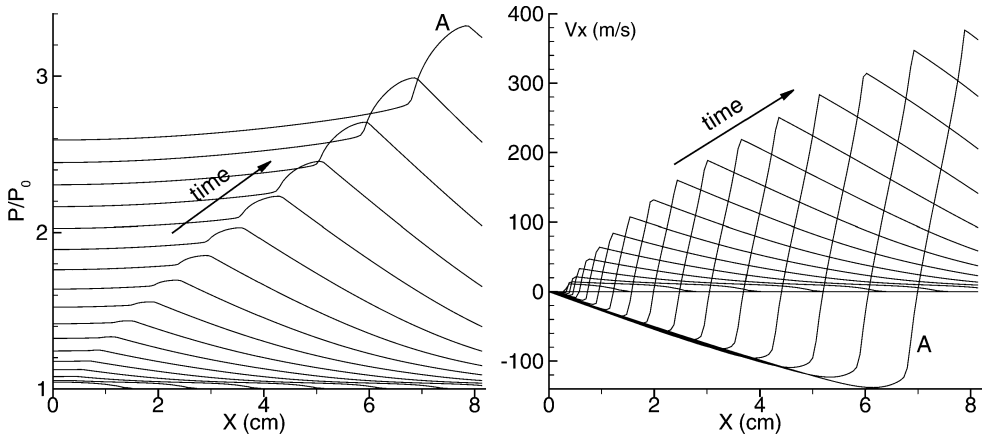

Fig. 6 Time sequence of pressure and longitudinal velocity profiles at the symmetry line of a two-dimensional half-channel 8.192 × 0.032 cm. Time changes from 0 to 5.66 × 10^{-4} s with increment (2.5–3.5) × 10^{-6} s between profiles. Profiles A correspond to 5.66 × 10^{-4} s.

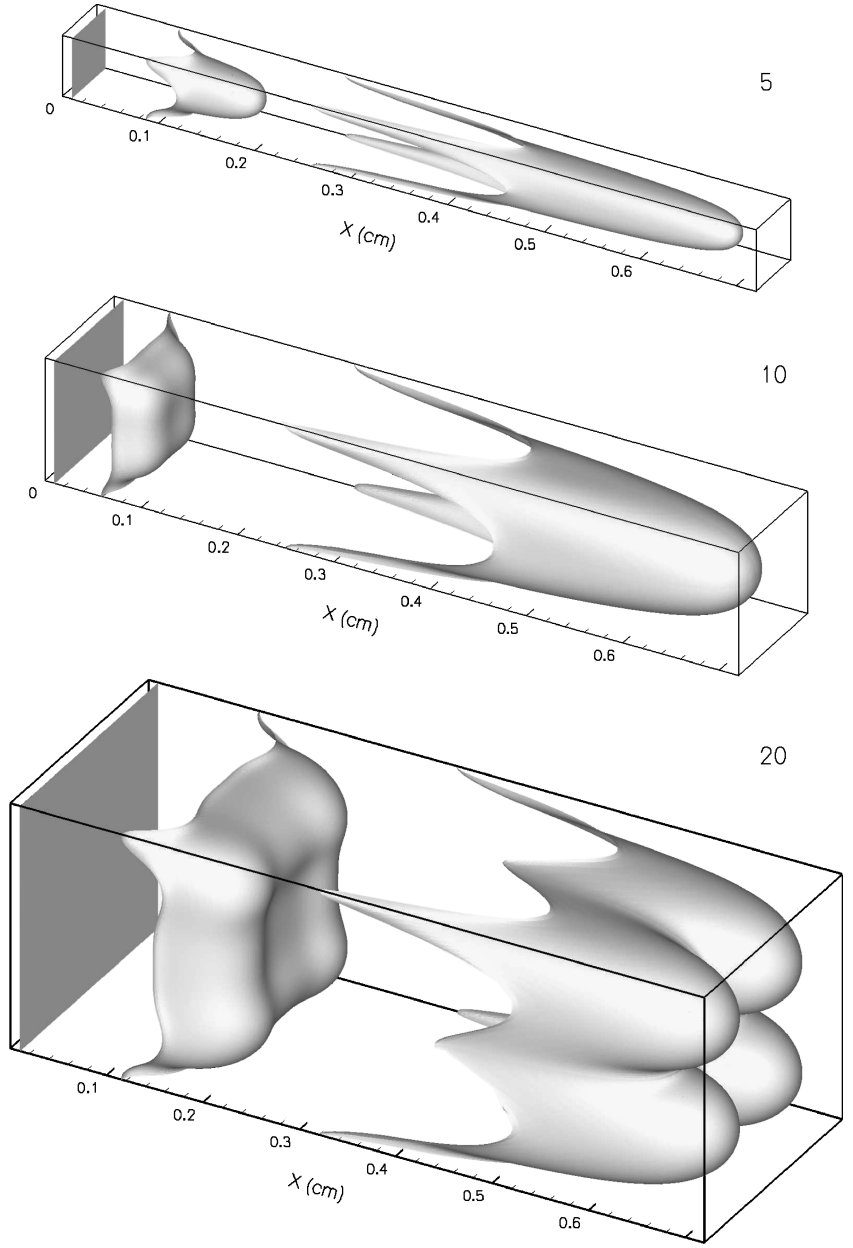

Fig. 7 Evolution of the flame surface in full three-dimensional channels of different widths and $L = 1.024$ cm. Numbers 5, 10, and 20 are scaled channel widths d/x_l. Flame surfaces are shown at 0, 0.98 × 10^{-4}, and 1.59 × 10^{-4} s for $d/x_l = 5$; at 0, 0.74 × 10^{-4}, and 2.19 × 10^{-4} s for $d/x_l = 10$; and at 0, 1.50 × 10^{-4}, and 2.97 × 10^{-4} s for $d/x_l = 20$.

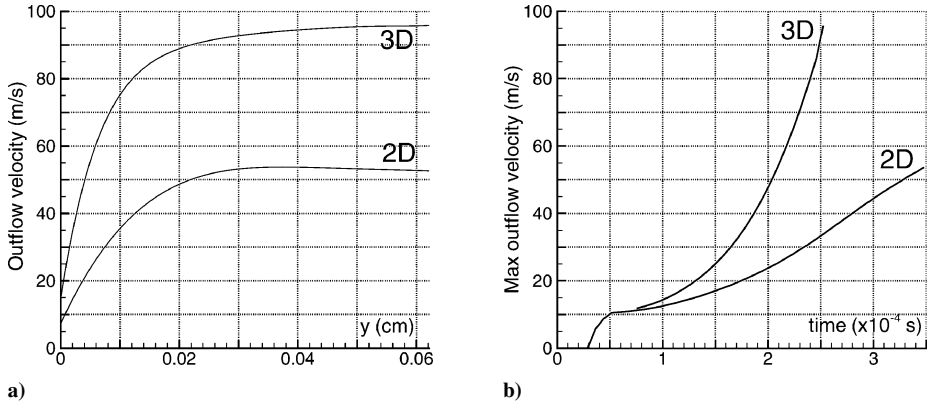

a) b)

Fig. 8 Outflow velocities computed for two- and three-dimensional channels: a) outflow velocity profiles at the time when the flame reaches the open boundary and b) maximum outflow velocity as a function of time. The channel length is 1.024 cm, and the channel half-width is 0.064 cm ($d/x_l = 10$). The three-dimensional velocity profile is shown for the symmetry plane. Maximum velocities in plots a and b are the same.

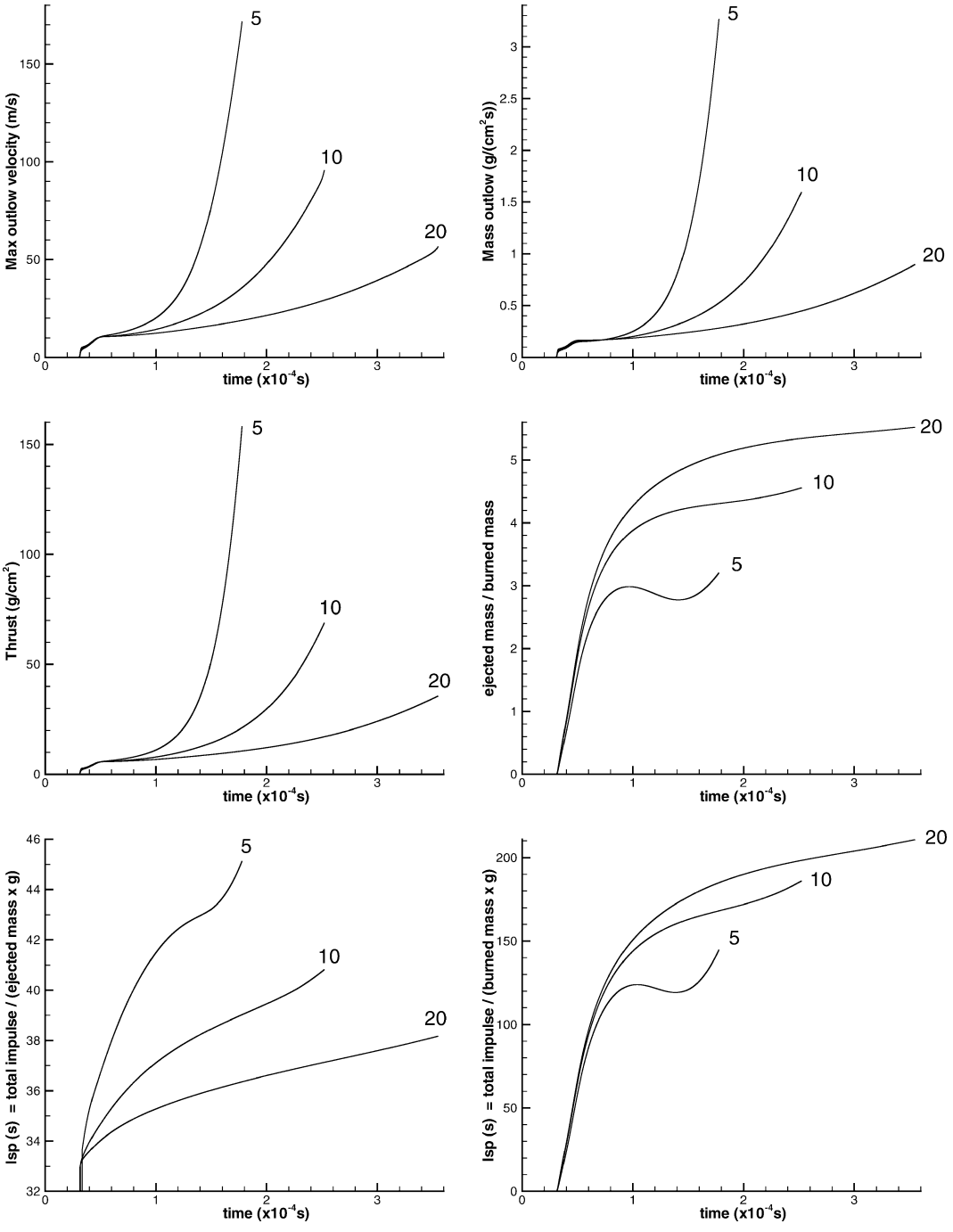

Fig. 9 Integral propulsion characteristics calculated for 1.024-cm-long three-dimensional channels. Numbers 5, 10, and 20 are scaled channel widths.

the narrowest channel ($d/x_l = 5$), the initially planar flame surface becomes convex in the middle of the channel shortly after the ignition. As the flow accelerates and interacts with boundaries, the flame stretches along the channel, so its shape roughly mimics the longitudinal velocity profile. For a larger channel ($d/x_l = 10$), the flame surface becomes slightly concave in the middle of the channel, and then quickly develop a regular convex shape. For the largest channel ($d/x_l = 20$), the flame surface develops a concave cavity in the vicinity of symmetry planes that remains until the flame reaches the end of the channel. Similar concave flames were observed in two-dimensional simulations and analyzed in Ref. 1. They appear at initial stages of flame development in larger channels, when the boundary layer thickness is small compared to the channel width, and disappear with time if the channel is long enough.

The flame and the flow acceleration in three-dimensional channels is significantly more efficient than that in two-dimensional channels

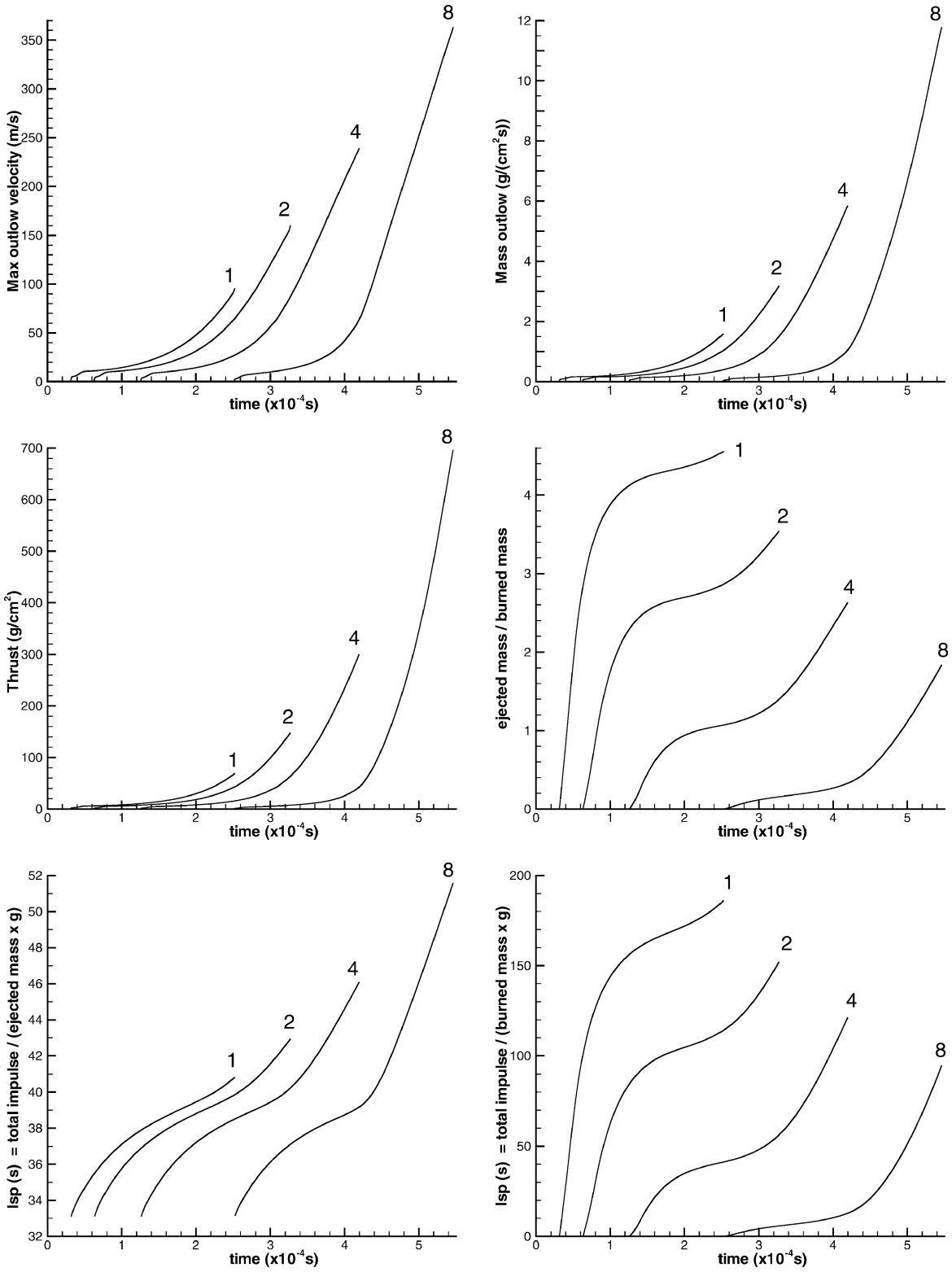

Fig. 10 Integral propulsion characteristics calculated for channel half-width 0.064 cm (d/x_l = 10). Numbers 1, 2, 4, and 8 correspond to channel lengths 1.024, 2.048, 4.096, and 8.192 cm.

due to the additional boundary-layer effect of side walls in the third dimension. The surface area of a flame distorted in three dimensions grows faster than in the two-dimensional case, thus causing a faster increase of the energy release rate and the flow velocity. Figures 5 and 8 show that the maximum outflow velocity reached in three-dimensional channels was up to two times higher than that in two-dimensional channels of the same size.

The outflow velocity as a function of distance from the no-slip wall is shown in Fig. 8a for two- and three-dimensional cases at the time when the flame reaches the open end of the channel. The two-dimensional profile is a little flatter in the middle of the channel than the three-dimensional profile, but in both cases the outflow speed is high across a substantial part of the channel cross-section ($\sim$0.7 for two-dimensional and $\sim$0.5 for three-dimensional), thus providing significant thrust.

The integral propulsion characteristics calculated for three-dimensional channels of fixed channel length, 1.024 cm, and variable cross-sections are summarized in Fig. 9. The quantities shown are the maximum outflow velocity, mass outflow, trust, ratio of the ejected mass to the burned mass, and the specific impulse I_{sp} defined in two different ways (as discussed in the next section). This figure shows, in particular, that the maximum outflow velocity, the mass outlow, and the thrust are approximately proportional to each other. The maximum thrust was obtained for $d/2 = 0.032$ cm ($d/x_l = 5$) and reached 158 g/cm^2 (or 0.65 g for the full channel) by the time the outflow velocity reached 172 m/s and the flame approached the open end of the channel. The corresponding ratio of the thrust to the initial mass of the material in the channel is about 10^6.

Figure 10 shows the same integral propulsion characteristics, but for a constant channel half-width $d/2 = 0.064$ cm ($d/x_l = 10$) and four channel lengths: 1.024, 2.048, 4.096, and 8.192 cm. This figure shows that at a fixed physical time, the outlow velocity in a longer channel is lower than in a shorter channel. There are three reasons for this. First, the mass of the unburned material accelerated ahead of the flame is larger for longer channels. Second, additional viscous losses in longer channels slow the flow acceleration. Finally, it takes longer for compression waves to reach the outflow boundary in a longer channel. In longer channels, however, the flame interacting with the boundary layer has more time to develop and eventually burns more material at higher rate. Outflow velocities compared at the times when flame reaches the open end of each channel increase dramatically with the channel length. Figure 10 shows that, when the channel length increases from 1.024 to 8.192 cm, the maximum outlow velocity increases from 95 to 360 m/s, and the maximum thrust increases from 70 to 700 g/cm^2.

To analyze the evolution of the burning rate in three-dimensional simulations, we computed the flame surface area S_F and the total energy generation rate W_q. Figure 11 shows the scaled values S_F/S_F^0 and W_q/W_q^0 as functions of time for all three-dimensional cases, where S_F^0 is the channel cross-section area, and W_q^0 is the energy release rate at the beginning of each simulation. The figure shows that for channels of different lengths and the same width ($d/x_l = 10$), the curves practically coincide for their effective time intervals. That is, the flame evolution is independent of the channel length. The figure also shows that the total energy generation rate increases mostly because of the increase in the flame surface area. For example, by 5×10^{-4} s, S_F/S_F^0 increases from 1 to 30, and W_q/W_q^0 increases from 1 to 90. This means that W_q increases by a factor of 30 because of the growth of the flame surface, and by another factor of 3 because of the increase of the burning rate per unit of the flame surface area. The burning rate increases because of the pressure increase, which is greater for faster flows.

V. Discussion

One interesting feature of the model propulsion device that we consider here is that the expanding burning products accelerate and eject unburned material ahead of the flame, so the mass of ejected material can be larger than the mass of burned material. For example, Fig. 9 shows that the ratio of the ejected mass to the burned mass for 1.024 cm long channels varies from 3 to 5.5. In a practical device, the ejected material does not have to be an unburned reactive mixture. It can be replaced by an inert gas if the device operates in a single-shot mode, or by combustion products from a previous cycle if the device operates in a cyclic mode. This leads to several possible definitions of the specific impulse (I_{sp}). Here we use two of them: I_{sp} as a total impulse scaled by an ejected mass, and I_{sp} as a total impulse scaled by a burned mass. Both of these I_{sp} are shown in Figs. 9 and 10. For 1.024-cm-long channels (Fig. 9), the maximum I_{sp} related to the ejected mass varies between 38 and 45 s. The maximum I_{sp} related to the burned mass varies between 145 and 210 s, according to the ratio of the ejected mass to the burned mass. When the channel length increases from 1.024 to 8.192 cm (see Fig. 10), the I_{sp} scaled by ejected mass increases from 41 to 52 s, but the I_{sp} scaled by burned mass decreases from 185 s to 95 s because the ratio of the ejected mass to the burned mass decreases from 4.6 to 1.8.

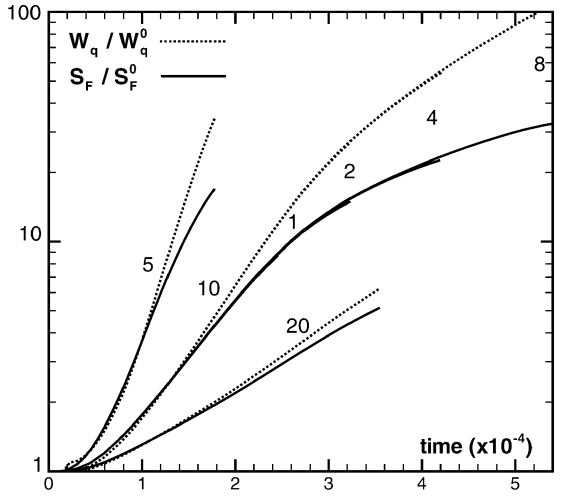

Fig. 11 Scaled flame surface area S_F/S_F^0 and total energy generation rate W_q/W_q^0 as functions of time for all three-dimensional cases shown in Figs. 9 and 10. Numbers 5, 10, and 20 are scaled channel widths d/x_l for 1.024-cm-long channels. Numbers 1, 2, 4, and 8 correspond to channel lengths 1.024, 2.048, 4.096, and 8.192 cm for 0.064-cm-wide channels ($d/x_l = 10$). Numbers 1, 2, 4, and 8 are located at the ends of the corresponding curves, which practically coincide for their effective time intervals. The scales S_F^0 and W_q^0 correspond to the planar laminar flame.

Numerical results presented here were obtained for idealized narrow channels with adiabatic walls. In practical systems, heat losses to the walls may decrease the flame acceleration, cause flame oscillations, and prevent flame propagation in very narrow channels. On the other hand, laminar flames accelerating in larger channels eventually become turbulent. Therefore, there is a limited range of experimental parameters for which the laminar flame acceleration induced by the boundary-layer effect can be observed. For example, experimental propane–air flames[16] observed in $109 \times 2.4 \times 2.4$ cm channels look laminar for the first 30–40 cm, develop a shape similar to that shown in Fig. 2, and accelerate to about 50 m/s for a stoichiometric mixture before the turbulence develops.

VI. Summary

Multidimensional numerical simulations of a laminar flame acceleration in narrow channels with adiabatic walls show that outflow velocities for these channels can reach hundreds of meters per second and provide a significant thrust. This can be achieved without creating strong shocks or detonations inside the channel. Because the material ahead of the flame is ejected without burning, the channel can be partially filled with an inert gas or combustion products from a previous pulse without affecting the energy release. Propulsion characteristics calculated for small channels filled with a reactive energetic mixture suggest that the laminar flame acceleration induced by boundary-layer effects can be used to create efficient micropropulsion devices.

Acknowledgments

This work was supported in part by the NASA Combustion Science and Chemically Reacting Systems Program (NRA 02-OBPR-03) and by the Naval Research Laboratory through the Office of Naval Research. Computing facilities were provided by the DOD HPCMP program. We thank Uday Hegde, Kurt Saksteder, and Richard Yetter for their comments and encouragement.

References

[1]Ott, J. D., "The Interaction of a Flame and Its Self-Induced Boundary Layer," Ph.D. Dissertation, Dept. of Aerospace Sciences, Univ. of Maryland, College Park, MD, 1999.

[2]Ott, J. D., Oran, E. S., and Anderson, J. D., Jr., "The Interaction of a Flame and Its Self-Induced Boundary Layer," NASA CR-1999-209401, Sept. 1999.

[3]Ott, J. D., Oran, E. S., and Anderson, J. D., "A Mechanism for Flame Acceleration in Narrow Tubes," *AIAA Journal*, Vol. 41, No. 7, 2003, pp. 1391–1396.

[4]Mallard, E., and Le Chatelier, H. L., "Recherches Expérimentales et Théoriques sur la Combustion des Mélanges Gazeux Explosifs," *Les Annales des Mines*, 8th Series, Vol. 4, 1883, pp. 274–376.

[5]Kerampran, S., Desbordes, D., and Veyssiére, B., "Study of the Mechanisms of Flame Acceleration in a Tube of Constant Cross-Section," *Combustion Science and Technology*, Vol. 158, 2000, pp. 71–83.

[6]Kerampran, S., Desbordes, D., Veyssiere, B., and Bauwens, L., "Flame Propagation in a Tube from Closed to Open End," AIAA Paper 2001-1082, Jan. 2001.

[7]Daou, J., and Matalon, M., "Flame Propagation in Poiseuille Flow Under Adiabatic Conditions," *Combustion and Flame,* Vol. 124, No. 3, 2001, pp. 337–349.

[8]Daou, J., and Matalon, M., "Influence of Conductive Heat-Losses on the Propagation of Premixed Flames in Channels," *Combustion and Flame*, Vol. 128, No. 4, 2002, pp. 321–339.

[9]Cui, C., Matalon, M., Jackson, T. L., "Pulsating Mode of Flame Propagation in Two-Dimensional Channels," *AIAA Journal*, Vol. 43, No. 6, 2005, pp. 1284–1292.

[10]Khokhlov, A. M., "Fully Threaded Tree Algorithms for Adaptive Refinement Fluid Dynamics Simulations," *Journal of Computational Physics*, Vol. 143, No. 2, 1998, pp. 519–543.

[11]Khokhlov, A. M., Oran, E. S., Chtchelkanova, A. Yu., and Wheeler, J. C., "Interaction of a Shock with a Sinusoidally Perturbed Flame," *Combustion and Flame*, Vol. 117, No. 1–2, 1999, pp. 99–116.

[12]Khokhlov, A. M., Oran, E. S., and Thomas, G. O., "Numerical Simulation of Deflagration-to-Detonation Transition: The Role of Shock-Flame Interactions in Turbulent Flames," *Combustion and Flame*, Vol. 117, No. 1–2, 1999, pp. 323–339.

[13]Khokhlov, A. M., and Oran, E. S., "Numerical Simulation of Detonation Initiation in a Flame Brush: The Role of Hot Spots," *Combustion and Flame*, Vol. 119, No. 4, 1999, pp. 400–416.

[14]Gamezo, V. N., Khokhlov, A. M., and Oran, E. S., "The Influence of Shock Bifurcations on Shock-Flame Interactions and DDT," *Combustion and Flame*, Vol. 126, No. 4, 2001, pp. 1810–1826.

[15]Oran, E. S., Gamezo, V. N., and Khokhlov, A. M., "Effects of Boundary Layers and Wakes on Shock-Flame Interactions and DDT," AIAA Paper 2002-0776, Jan. 2002.

[16]Schmidt, E. H. W., Steinicke, H., and Neubert, U., "Flame and Schlieren Photographs of Combustion Waves in Tubes," *Proceedings of the Combustion Institute*, Vol. 4, 1952, pp. 658–667.

H. Chelliah
Associate Editor